A 1D Bayesian inversion of microwave radiances using several radiative properties of solid hydrometeors

Marylis Barreyat, Philippe Chambon, Jean-françois Mahfouf, Ghislain Faure

Received: 29 April 2022 | Revised: 27 October 2022 | Accepted: 28 October 2022

DOI: 10.1002/asl.1142

RESEARCH ARTICLE

Atmospheric Science Letters RMetS

A 1D Bayesian inversion of microwave radiances using several radiative properties of solid hydrometeors

Marylis Barreyat | **Philippe Chambon** | **Jean-François Mahfouf** | **Ghislain Faure**

CNRM, Université de Toulouse, Météo-France, CNRS, Toulouse, France

Correspondence
Philippe Chambon, CNRM, Université de Toulouse, Météo-France, CNRS, Toulouse, France.
Email: philippe.chambon@meteo.fr

Funding information
Centre National d'Etudes Spatiales; Météo-France and Région Occitanie

Abstract

Numerical weather prediction centers increasingly make use of cloudy and rainy microwave radiances. Currently, the high microwave frequencies are simulated using simplified assumptions regarding the radiative properties of frozen hydrometeors. In particular, one single particle shape is often used for all precipitating frozen particles, all over the globe, and for all cloud types. In this paper, a multi-SSP (single scattering properties) approach for 1D Bayesian inversions is examined. Two experiments were set up: (1) one with three SSPs and (2) one with the previous SSPs plus one which leads to very cold brightness temperature distributions. For that purpose, we used observations from the GPM Microwave Imager radiometer over 2 months period and forecasts from the Météo-France convective scale AROME model. The results showed that mixtures of SSP are chosen by the inversion method for meteorological conditions with low scattering and that a single particle is chosen for those with high scattering to perform the inversions. Despite the fact that no specific weather scenes were found to be associated with a particular SSP the most efficient scattering particles can be favored for some of them.

KEYWORDS

cloud, hydrometeors, microwave, snow

1 | INTRODUCTION

In recent years, the exploitation of high microwave frequencies in cloudy sky conditions has significantly progressed both for numerical weather prediction (NWP) applications (e.g., Geer et al., 2017; Geer & Baordo, 2014) and for surface rain retrieval applications (e.g., Kidd et al., 2016, 2021). To improve the quality of the retrievals, many aspects of their treatment processes could be ameliorated like radiative transfer simulations. Similarly, for NWP models, this type of observation also requires the use of radiative transfer codes within which scattering properties parameterizations could also be improved in case of cloudy and/or rainy observations (Geer et al., 2017). Thanks to those codes, the NWP model brightness temperatures (Bts) are simulated according to a chosen frequency. Several micro-physical assumptions on solid hydrometeors, regarding the single scattering properties (SSPs), and the size distribution, are indeed required. Within current radiative transfer models, one single set of radiative properties has to be

Marylis Barreyat and Philippe Chambon contributed equally to this work.

selected in advance for each hydrometeor type. The resulting bulk properties (single scattering albedo, extinction, asymmetry, backscattering) are then stored in look-up tables as a function of hydrometeor content and temperature; these look-up tables are then to be further used within assimilation systems. Since high-frequency microwave radiances are sensitive to snowfall which can have a wide range of shapes, sizes, and densities, for example, an accurate SSP specification is crucial for optimal exploitation (Barreyat et al., 2021; Geer & Baordo, 2014; Kulie et al., 2010; Ringerud et al., 2019).

Currently, in most NWP centers exploiting cloudy and rainy radiances, the high microwave frequencies are simulated with a single "optimal" particle shape for snowfall. Several studies focused on searching for optimal particle radiative properties to fit the microwave observation distributions (e.g., Geer & Baordo, 2014; Guerbette et al., 2016; Haddad et al., 2015; Mangla et al., 2021). Optimizations including different solid hydrometeor properties have been investigated: in Geer (2021) a parameter estimation method is used in order to select an optimal shape for several species at the same time. Knowing the diversity of the possible solid hydrometeor characteristics (Hallett & Mason, 1958; Magono & Lee, 1966; Nakaya, 1954), this represents a huge simplification of the atmosphere despite the availability of databases providing scattering properties for many solid hydrometeors (Ding et al., 2017; Liu, 2008), ARTS (Brath et al., 2020; Eriksson et al., 2018; Kneifel et al., 2018). Several studies have investigated the use of ensembles of radiative properties, for a different part of the spectrum. Baran and Labonnote (2007) developed a model for cirrus clouds using a set of crystals to simulate brightness temperatures in the infrared range. Kulie et al. (2010) averaged radiative transfer simulations with the properties available in the databases of Liu (2008) and Hong (2007) to derive microwave brightness temperatures. Using this latter method within a precipitation retrieval algorithm (Kummerow et al., 2001; Randel et al., 2020; Ringerud et al., 2019) obtained positive improvements with the database of Liu (2008).

At Météo-France, the "1D-Bay+3D/4D-Var" scheme is operationally used to assimilate ground-based radar reflectivities since 2010 (Caumont et al., 2010; Wattrelot et al., 2014) and cloudy and/or rainy microwave radiances from the ATMS and MHS sounders since 2021 (Duruisseau et al., 2019). In order to consider the variability of solid hydrometeor, a method based on the first step of the "1D-Bay+3D/4D-Var" scheme, and choosing between mixtures of SSPs, has been developed to retrieve vertical profiles of relative humidity from cloudy and/or rainy observations. Unlike previously explored methods, the present one dynamically defines optimal radiative property ensembles using microwave observations as a priori information. The aim of this study is to examine the relevance of such a method to perform inversions of cloud and/or rainy microwave radiances. It is part of a research project aiming to take into account within data assimilation the variability of hydrometeor properties. Before performing an evaluation through data assimilation experiments, the particle choices within the revised 1D-Bayesian inversion scheme need to be documented. Therefore, our main objective is not yet to quantify the benefits of such a novel approach but to examine its potential in order to exploit it to the full afterward. The outcome of this study will be to provide guidance on how to exploit scattering property databases more efficiently in a data assimilation framework.

Section 2 describes the NWP system and the observations used in this paper to conduct experiments with the 1D Bayesian inversion scheme. The experiments and the products selected to evaluate the results are introduced in Section 3. In Section 4 results from the experiments are presented and discussed. Finally, conclusions drawn from this study are summarized in Section 5.

2 | GPM MICROWAVE IMAGER DATA AND NWP SYSTEM

The experiments with different mixtures of SSPs have been conducted over a 2-month period using Bts from level 1B products from the GPM Microwave Imager (GMI L1B ATBD, 2016) within a ±90 min time window around the time of validity of 3-h forecasts of the Application of Research to Operations at Mesoscale (AROME)-Antilles NWP model (Faure et al., 2020). This convective scale model, with a resolution of 2.5 km, is used operationally at Météo-France over several geographical domains in the Tropics including the Caribbean geographical area (10.4°N to 22.45°N; 67.8°W to 52.2°W). The microphysical scheme of this model generates prognostic cloud liquid water, cloud ice water, rain, snow, and graupel mixing ratios. We selected GMI Bts over a period of high convective activity from September 1, 2017 to October 31, 2017. This instrument was chosen because of its wide range of frequencies from 10.65 GHz to 183.31 ± 7 GHz. Due to different channel footprint sizes across frequencies, the raw Level 1B data were superobbed onto a regular lat/lon grid at 0.1° resolution. Considering the fact that numerical models have an effective resolution three to four times larger than their actual grid (Ricard et al., 2013), this resolution for superobbing is therefore compatible with one of the AROME-Antilles models. Then, the GMI Bts were simulated with version 12 of the Radiative Transfer for TIROS Operational Vertical sounder code RTTOV-SCATT (Saunders et al., 2018).

This code, based on the Delta-Eddington approximation, needs, among other parameters, the bulk scattering properties of the hydrometeors. These bulk properties are computed by integrating the SSPs over particle sizes using a particle size distribution (PSD). An important feature is that the particle mass needs to be defined as a function of the maximum dimension of the particle. This is done thanks to the particle mass-size function which depends on two coefficients. In this study, both coefficients are taken from table 1 of Kulie et al. (2010). Additionally, the RTTOV-SCATT version used in this study does not consider the graupel hydrometeor. Therefore, we summed the graupel content with the snow content generated by the forecast model. Finally, the chosen characteristics to describe the hydrometeors are:

- A Marshall–Palmer (Marshall & Palmer, 1948) PSD and a Mie sphere to simulate the rain;
- A (Field et al., 2007) tropical PSD and the 11 different shapes from Liu (2008) to simulate the snow;
- A modified gamma (Petty & Huang, 2011) PSD and a Mie sphere to simulate the cloud of liquid water;
- A modified gamma (Petty & Huang, 2011) PSD and a Mie sphere to simulate the cloud ice water.

3 | METHOD

3.1 | Experiment definition

A 1D Bayesian inversion has been developed at Météo-France to retrieve atmospheric profiles from cloudy microwave Bts (Barreyat et al., 2021; Duruisseau et al., 2019; Guerbette et al., 2016). The retrieved profiles are derived from a weighted average of profiles x_i in the neighborhood of a given observation y. A 250 × 250 km domain is chosen around each observation with profiles taken from an AROME short-range forecast (First-Guess [FG]). The largest weights are given to the simulated Bts closest to the observed ones. The retrieved profile is given by:

$$x_{ret} = \frac{\sum_{i=1}^{n} w_i x_i}{\sum_{i=1}^{n} w_i}$$

With

$$w_i = e^{\sum_{j=1}^{d} \left(-\frac{1}{2}\left[y_{o,j} - H_j(x_i) - b_j\right]^t R^{-1} \left[y_{o,j} - H_j(x_i) - b_j\right]\right)},$$

where i corresponds to a given profile in the inversion database (excluding the first guess), j is a given channel, d is the number of channels selected for the inversion, $H(.)$ is the observation operator, R the covariance matrix of observation errors and b_j is a clear-sky bias correction between the FG and the observations previously computed for all GMI frequencies over a 2-month period. In order to process the largest possible number of inversions, the accepted weight threshold has been set to 10^{-200}. If this threshold is exceeded, it leads to a successful inversion.

In the 1D Bayesian inversion developed for the present study, instead of simulating a set of d channels for each observation, we consider additional Bts, where m is the number of radiative configurations selected in the radiative transfer model RTTOV-SCATT. Each specification of SSP leads to a change of the PSD free parameter to compute the bulk scattering properties. However, for simplicity, the following results coming from bulk scattering property changes are commented as coming from SSP changes. Therefore, each retrieved profile is written as:

$$x_{ret} = \frac{\sum_{i=1}^{n}\sum_{k=1}^{m} w_{i,k} x_i}{\sum_{i=1}^{n}\sum_{k=1}^{m} w_{i,k}}$$

with

$$w_{i,k} = e^{\sum_{j=1}^{d} \left(-\frac{1}{2}\left[y_{o,j} - H_{j,k}(x_i) - b_j\right]^t R^{-1} \left[y_{o,j} - H_{j,k}(x_i) - b_j\right]\right)}.$$

For each inversion, we computed the normalized inversion weights for a given SSP. In this paper, the inversions having a normalized inversion weight greater than 0.95 for one SSP are considered as using a "single SSP" to perform the inversions. In other cases, the inversions are considered as using a mixture of SSPs. To assess the impact of using various SSPs within the Bayesian inversion, the method is first tested by changing only snowfall radiative properties, since this hydrometeor has a wide diversity of shapes and densities that strongly impact Bts at high frequencies. Two experiments using different sets of SSPs have been set up to examine (i) if the method favors the use of mixtures against the use of a single SSP with a set of SSPs generating moderate scattering and (ii) if the introduction of an "outlier" SSP, generating a lot of scattering on top of the latter set, has an influence on the results.

The first experiment is performed with 3 SSPs from the Liu (2008) database. These SSPs are Sector snowflake, Rosette 6-bullet, and Rosette 3-bullet. This choice was motivated by their Bt distributions simulated with the AROME-Antilles model which are close

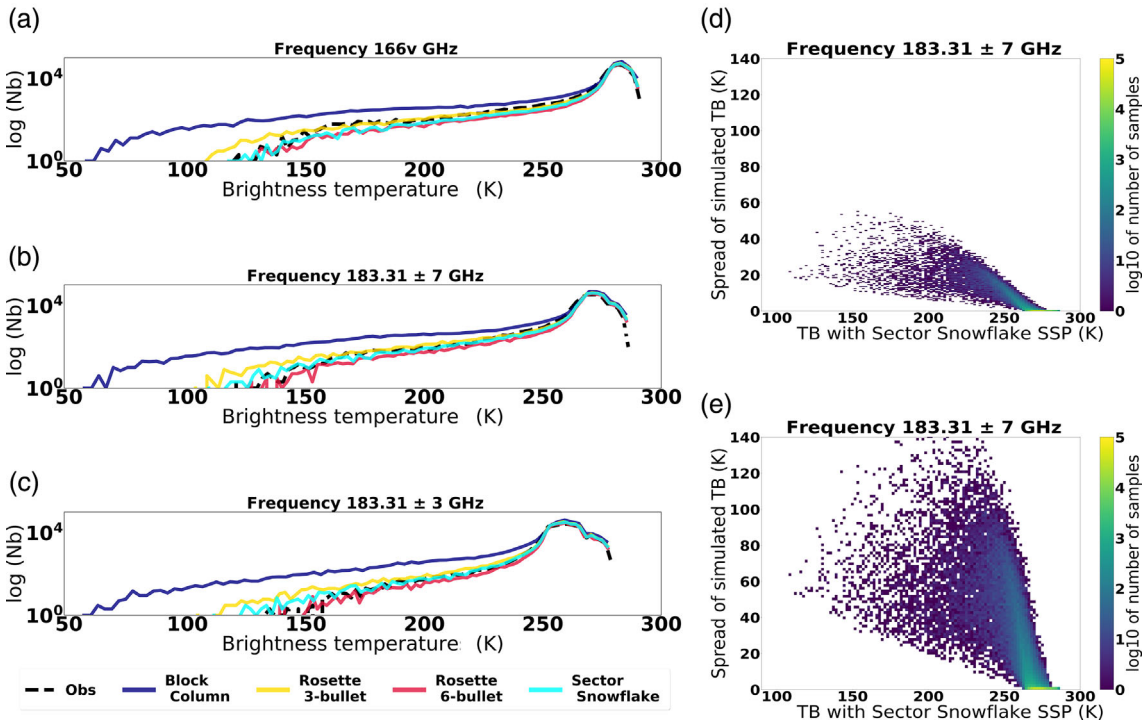

FIGURE 1 (a–c) FG simulated Bt distributions respectively at frequencies 166v, 183.31 ± 7, and 183.31 ± 3 GHz for a 2-month period. (d, e) Scatter plots of the spread between the minimum and the maximum simulated Bts respectively for 3 and 4 SSPs at 183.31 ± 7 GHz frequency for a 2-month period

to the observed ones, as shown in Figure 1a–c. In order to highlight the variability of the simulated Bts depending on particles for the two experiments, the distributions of their differences in simulations are plotted at the frequency 183.31 ± 7 GHz (Figure 1d,e). This frequency is interesting due to its sensitivity to scattering signals produced by ice particles. However, despite similarities in Bt distributions for the three SSPs (Figure 1a–c), Bts simulated with the Sector snowflake can be up to 50 K different from the two other particles (e.g., Figure 1d).

For the second experiment, the Bayesian inversion is performed with 4 SSPs. On top of three SSPs from the first experiment, the block column SSP is added. This particle, generating more scattering than the other ones, very low Bt values can be simulated (down to 50 K) as shown in Figure 1a–c. Given the differences in observations, the Block column particle is obviously not a particle that one would use a priori as a single particle shape within a data assimilation experiment. The motivation here is to check if this particle shape could still be useful in some specific meteorological situations. Figure 1e shows the spread between the 4 SSPs, and it can be seen that the differences are much larger than in Figure 1d with only 3 SSPs. Indeed, the spread reaches up to 140 K since with the Block Column particle Bts can be very low.

3.2 | Result evaluation metrics

The multi-SSP inversion allows us to identify, for each retrieved profile, which particles are used with their associated weights. This aspect is examined in the following to understand the behavior of the method. Objectively assessing the quality of the retrievals with multiple particles with respect to a single particle retrieval is a difficult task. One possibility is to examine the number of successful inversions in each case, a larger number indicating a better fit to observations. Another possibility is to run the radiative transfer with retrieved profiles to examine the fit of the retrievals in the observation space. But this means specifying a particular SSP within the RTTOV-SCATT model to simulate the Bts. We will see in the following the pros and the cons of this method.

The results of both experiments have been categorized according to three predictors. The aim of this investigation is to check whether a given particle shape is more frequently used depending on the weather scene and on its scattering properties. The first two predictors are the surface precipitation and the ice water path from the GPM GMI (GPROF) Radiometer Precipitation Profiling L2A 1.5 hours 13 km V05 products collocated with GMI Bts on the regular lat/lon 0.1° grid. The last one is an index

characterizing the scattering intensity of the weather scenes. This index, originally designed to detect precipitation, is calculated from 18.7v, 23.8v, and 89v GHz frequencies (Grody, 1991; Wilheit et al., 2003). Its expression is given by:

$$P_{SI} = 451.9 - 0.44Bt^{18.7v} - 1.775Bt^{23.8v} + 0.00575\left(Bt^{23.8v}\right)^2 - Bt^{89v}.$$

Finally, in order to select only the cloudy and rainy profiles in the observations (so called "cloudy observations" in the following) to perform the inversions, the sample profiles were selected according to

1. a P_{SI} index >5 K;
2. a surface precipitation amount >0.1 mm/h;
3. an ice water path amount >0.1 kg/m^2.

4 | EXPERIMENTS

In this section, a case study is first chosen to examine the behavior of the multi-SSP 1D Bayesian inversion and to illustrate it in detail. Then, the method is investigated thanks to a statistical study over a 2-month convective period.

The selected case study is associated with the tropical cyclone Maria which developed over the Caribbean sea in September 2017.

4.1 | Case study

Figure 2a,b display respectively the cyclone Maria observed at 183.31 ± 7 GHz by GMI and simulated by the AROME-Antilles model at 3 UTC on September 22, 2017. Despite a good agreement in terms of shape for the main

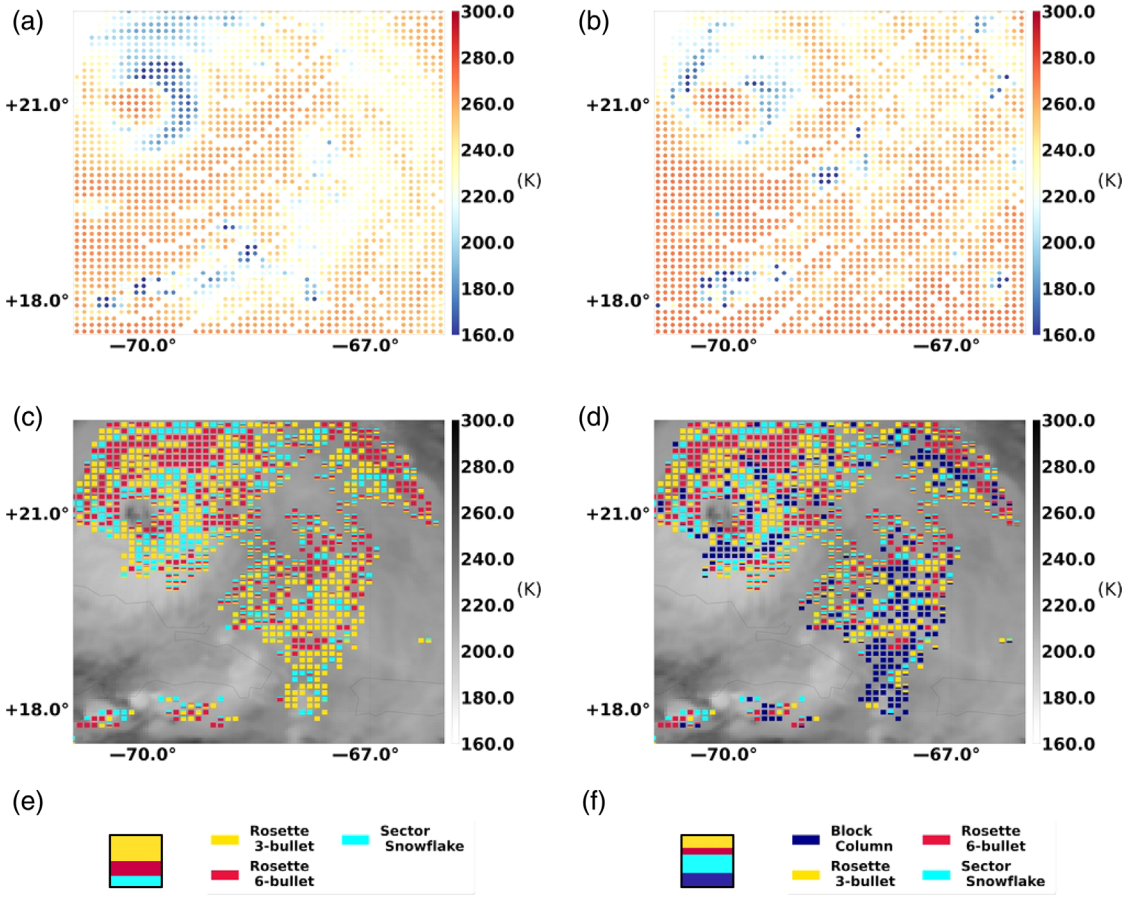

FIGURE 2 (a) GMI observations of the Maria cyclone reaching the West Indies on September 22, 2017 for the 183.31 ± 7 GHz frequency. (b) FG simulated Bt simulations of the cyclone for the same frequency with the Sector snowflake SSP. (c, d) Normalized inversion weights for profiles characterized as cloudy and rainy by the criteria defined in Section 3.2 with respectively the 3 SSPs (Rosette 3-bullet in yellow, Rosette 6-bullet in red and Sector snowflake in cyan) and the 4 SSPs (the 3 SSPs plus block column in dark blue) with observed infrared imagery at frequency 10.3 μm as background. Each square-colored block represents one Bayesian inversion, and within each square, the colored areas represent the normalized inversion weights of each SSP. (e, f) Examples of normalized inversion weights respectively for the 3 SSPs and 4 SSPs experiments

patterns, the cold Bts around the eye of the cyclone are not located at the same place in the observations and in the FG.

First, we performed the Bayesian inversion allowing a mixture of SSPs with 3 and 4 particles and verified that the weather structures found using the simulated Bts of the retrieved profiles were consistent with the observed ones (not shown). The corresponding weights are shown in Figure 2c,d. It appears that either a mixture of SSPs or a single SSP was used (normalized inversion weights of one SSP greater than 0.95). The Rosette 3-bullet and Rosette 6-bullet are chosen over specific areas (leading to geographically consistent patterns) whereas the Sector snowflake selection is more patchy. However, the particle choice cannot always be interpreted as a function of observation location within the cyclone (e.g., close to the core or within a spiral band). The addition of the Block column particle reduces the use of the Rosette 3-bullet particle in particular inside the south spiral band of the cyclone.

4.2 | Statistical study

After this qualitative assessment of the multi-SSP approach, results over 2 months (from September to October 2017) are examined using statistical diagnostics. The 3SSP and 4SSP experiments are both compared with another experiment (1SSP). The latter experiment corresponds to a 1D-Bayesian inversion using only the Sector snowflake particle to perform the inversions, which means that no mixtures can be used. The particle choice was motivated by its use in the Météo-France operational system following studies at ECMWF (Geer & Baordo, 2014). Out of a total number of 8537 cloudy observations over the domain and during the period of the study, the number of successful inversions for each experiment is respectively 8238, 8366, and 8425 for the 1SSP, 3SSP, and 4SSP experiments. It can be seen that this number increases with the number of SSPs taken into account.

The standard deviations of differences between analyzed Bts and observations have been computed for the three experiments over a 2-month period and for each GMI frequency used in this study. The relative differences between the standard deviations of the 3 and 4SSPs experiments with respect to the 1SSP experiment are displayed in Figure 3. One can see that for channels 10 to 13, which are the most affected by the specification of snow radiative properties; there is an apparent degradation of the analysis fit to the observations for both the 3 and 4SSPs experiments. However, for channels 3 to 9, which are the channels less sensitive to this specification, the results show significant improvements. Indeed, as mentioned above, rerunning the radiative transfer onto the analyzed profiles is inevitable to take into account the non-linearities of simulations. In this study, the Sector Snowflake was used to rerun the simulations for the three experiments. Hence one interpretation of the degradation of channels 10 to 13 is that the latter assumption artificially favors the 1SSP experiment. Therefore, even though the improvements of channels 3 to 9 analysis fits seem encouraging, this method of evaluation should be taken with caution in particular for the high-frequency results. Another way to evaluate the results would be to compute newly analyzed Bts as the weighted sum of background Bts. Using these analyzed Bts would be an alternative diagnostic to the one shown above to deepen the understanding of the radiative transfer simulations. The disadvantage of this latter diagnostic is that it would not take into account the non-linearities of the radiative transfer with respect to the hydrometeor content. At last, a one-third-option of diagnostic would be to compute specific hydrotables for each profile, taking into account the weights of each particle shape into the bulk radiative properties, and rerun the non-linear radiative transfer with those tailored hydrotables for each profile. However, this latter diagnostic would be computationally intensive to set up.

The distributions of weights of the cloud and/or precipitation profiles are displayed using violin plot diagrams (Barton et al., 2021; Riccardi et al., 2021; Thrun et al., 2020) as shown in Figure 4. Thanks to their representation of the probability density for each value of the distribution, these diagrams have the advantage of being able to represent multimodal distributions, unlike box plot diagrams. In this statistical study, we considered only cloudy and rainy observations defined by the three predictors in Section 3.2.

In Figure 4a–f, the particle weights are characterized by multimodal distributions with one mode towards 0 and another one towards 1. The Rosette 3-bullet, and more particularly the Rosette 6-bullet and the Sector snowflake particles have their distribution widening around 33% which means that they are selected within mixtures. The addition of the Block column particle in Figure 4f reduces the weights close to 1 of the Rosette 3-bullet particle in agreement with Figure 3d. The Rosette 3-bullet being the SSP generating the strongest scattering after the Block Column among the four selected particles, it appears that some weather scenes required increased diffusion in RTTOV-SCATT to match observed Bts. Indeed, the Block Column particle weights which are different from 0 are all close to one. This indicates that this particle is not used within mixtures but individually for weather scenes that cannot be well

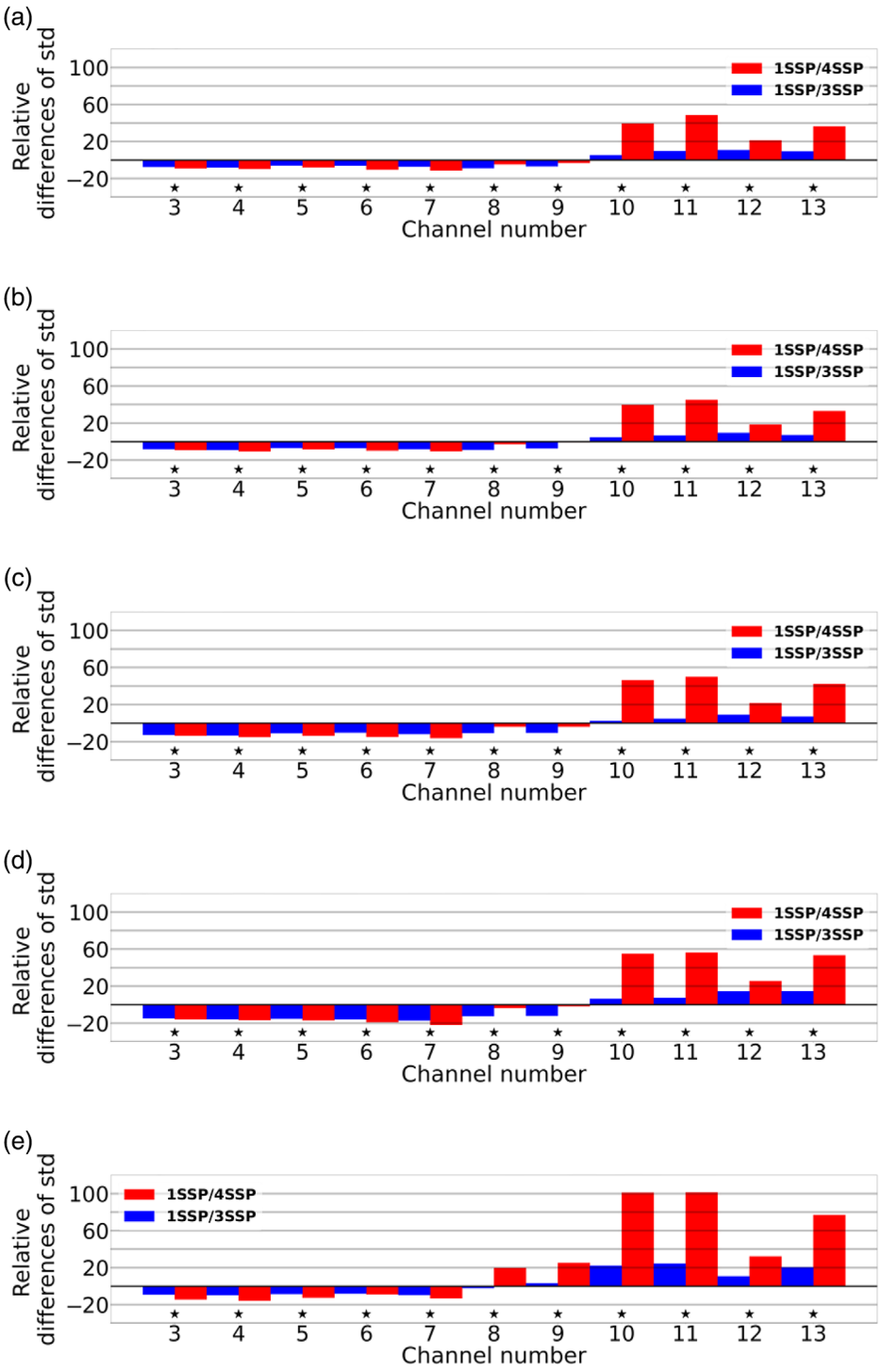

FIGURE 3 Relative differences of standard deviations of the analyzed Bts minus observations between the 3SSP and 1SSP (blue) or between the 4SSP and 1SSP (red) experiments over a 2-month period for each GMI channel used. Stars indicate that the differences in standard deviations are significant at the 95% level. (a) Sample with scattering index range: 5 and 10 K. (b) Sample with scattering index range: 10 and 15 K. (c) Sample with scattering index range: 15 and 20 K. (d) Sample with scattering index range: 20 and 25 K. (e) Sample with scattering index range: 25 K and +

simulated with other particles. Indeed, some SSPs do not allow model simulations to reach sufficiently low Bts, which can be achieved using the Block column particle.

It could also come from a lack of hydrometeor contents within the model forecast and therefore compensating for a model bias. A related bias on surface precipitation of the AROME-Antilles model has been brought out in Faure et al. (2020) thanks to an independent evaluation of precipitation forecast with respect to satellite rainfall products. Further diagnostics, like cross-validations with other instruments, would then need to be performed to understand if this behavior is the result of model biases or observation operator biases.

It also appears in Figure 4 that the weights are increasingly close to 0 or 1 as the P_{SI} index increases which means that the mixtures are gradually decreasing as the weather situation leads to more scattering.

The means of the distributions give information about the percentage of use of each particle as a function of the P_{SI} index. We observe that the means are not changing a

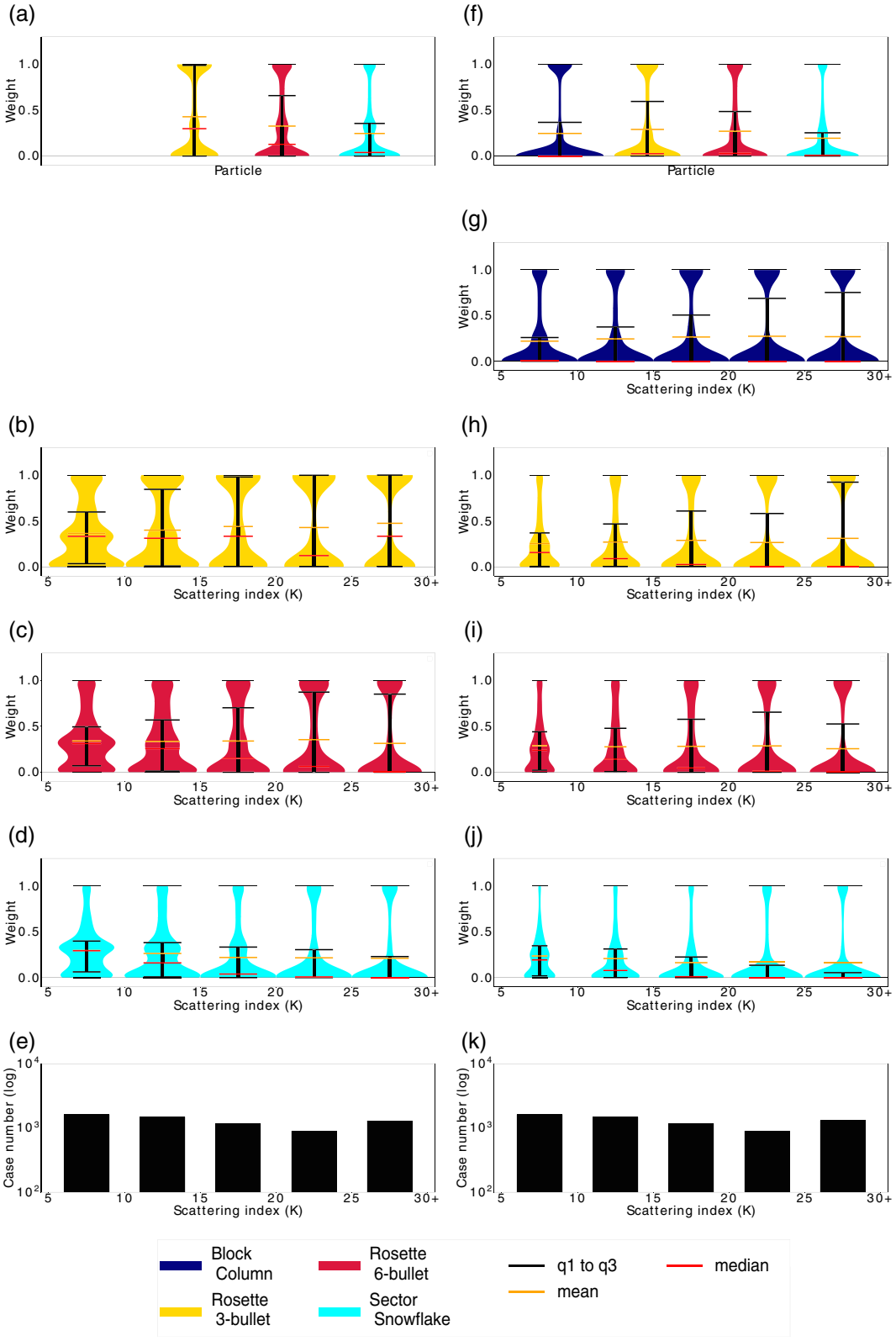

FIGURE 4 (a) Violin plots of the cloudy observation distributions, according to criteria defined in Section 3.2, for each SSP over the 2-month period with the 3 SSPs experiment. (f) Same with the 4 SSPs experiment. (b–d) Violin plots of the cloudy observation distributions over the 2-month period with respect to the P_{SI} index of the 3 SSPs experiment respectively for Rosette 3-bullet, Rosette 6-bullet, and Sector snowflake. (g–j) Same with the 4 SSPs experiment respectively for Block column, Rosette 3-bullet, Rosette 6-bullet, and Sector snowflake. (e) Histogram of the number of cloudy observations per bins of P_{SI} index for the 3 SSPs experiment. (k) Same with the 4 SSPs experiment

TABLE 1 Percentage of use between mixtures and single SSP within the 1D-Bayesian inversion over a 2-month period as a function of 3 predictors respectively surface precipitation, P_{SI} scattering index, and ice water path for the 3SSP (4SSP) experiments

Surface precipitation					
Bin (mm/h)	[0.1;2]	[2;10]	[10;25]	[25;+]	
Mixture (%)	55 (55)	38 (37)	24 (25)	24 (22)	
Single SSP (%)	45 (45)	62 (63)	76 (75)	76 (78)	
P_{SI}					
Bin (K)	[5;10]	[10;15]	[15;20]	[20;25]	[25;+]
Mixture (%)	78 (76)	68 (67)	51 (51)	37 (38)	26 (27)
Single SSP (%)	22 (24)	32 (33)	49 (49)	63 (62)	74 (73)
Ice water path					
Bin (kg/m^2)	[0.1;0.5]	[0.5;1]	[1;2]	[2;+]	
Mixture (%)	68 (67)	42 (43)	22 (22)	17 (18)	
Single SSP (%)	32 (33)	58 (57)	78 (78)	83 (82)	

Note: The use of a single SSP is defined when one of the SSPs has a normalized weight larger than 0.95.

lot across the range of scattering indices for both experiments, except for the Sector snowflake particle: the mean slightly decreases with the increase of the latter for the two experiments. Nonetheless, no single SSP is clearly predominant over the others according to the P_{SI} intervals. Thus, it seems difficult here to choose a preferred SSP according to the P_{SI} index.

In addition, we computed the percentage of usage for each particle within the 1D-Bayesian inversion for the 2-month period for both experiments. It appeared that for the 3SSP experiment the most used particle was the Rosette 3-bullet one with a percentage of 43%. The other percentages are equal to 33% and 24% respectively for the Rosette 6-bullet and the Sector snowflake particles. The results for the 4SSP experiment are 25%, 29%, 27%, and 19%, respectively for the Block column, the Rosette 3-bullet, the Rosette 6-bullet, and the Sector snowflake particles. In both experiments, the Rosette 3-bullet is therefore selected more frequently than the others and the Block column ends up being used a significant number of times despite being an outlier particle in the sense of Figure 1 distributions.

Table 1 reveals that the percentage of mixtures is reduced as the P_{SI} index increases, in agreement with our previous findings. If we look at the 3SSP results, from 78% for a P_{SI} index between 5 and 10 K, the fraction of mixture decreases to 26% for a P_{SI} index above 25 K. We then examined this behavior with the two other predictors. A similar behavior is noticed for the other predictors. From 55% of mixtures for surface precipitation between 0.1 and 2 mm/h, this fraction is reduced to 24% for surface precipitation above 25 mm/h. Similarly from 68% for ice water path amounts ranging between 0.1 kg/m^2 and 0.5 kg/m^2, the percentage decreases to 17% for ice water path amounts above 2 kg/m^2. The percentages with the 4SSP experiment lead to similar conclusions: the use of a single particle increases along with the surface precipitation, the P_{SI} index, and the ice water path. This indicates that highly scattering weather scenes are frequently well simulated by a single SSP in the Bayesian inversion. This is in contrast to weakly scattering scenes which can be often simulated accurately by a mixture of particles. This can be explained by the simulated Bt distributions of the SSPs which have their largest differences for highly scattering weather scenes. This leads to important differences in simulated neighborhood Bt profiles. Thus, for these cases, only one SSP (associated with a lot of scattering) is useful to reach values close to observations. On the contrary, for an observation that contains few hydrometeors, the method simulates Bts that differ only slightly among various SSPs. Thus, the inversion can assign an almost identical weight to each SSP and create a mixture.

Overall, both results reveal that the mixtures are as frequently chosen as a single particle within the Bayesian inversion. However, they are dominant for low scattering situations whereas a single particle is more frequently selected in highest scattering situations.

5 | CONCLUSIONS

This study examined the interest in using several radiative properties for solid hydrometeors within a 1D Bayesian inversion of microwave brightness temperatures. Our motivations came from the strong sensitivity of radiative transfer simulations at high frequencies to scattering properties of hydrometeors and from the need to overcome some limitations of the choice of a single "optimal" particle. For that purpose, atmospheric profiles from the convective scale model AROME Antilles and brightness temperatures between 18 and 183 GHz from the microwave radiometer GMI onboard the GPM-Core satellite have been considered. Results have been examined for a case study (hurricane Maria) and over a 2-month period (September–October 2019). A revised Bayesian inversion

has been assessed using a number of SSPs from the Liu (2008) database with two experiments: one with 3 SSPs leading to simulated Bt distributions with the AROME model close to the GMI one; and another one with the 3 previous SSPs plus one with a distribution characterized by a larger tail of low Bts compared to observations. As the inversion can choose among a mixture of SSPs to perform the inversion, we examined carefully how the weights for each particle were distributed.

The case study highlighted the usefulness of each SSP in the inversions by excluding none of them. In the second experiment, adding the Block Column SSP on top of the 3 SSPs, showed the usefulness of an SSP generating further scattering leading to a larger number of successful inversions. Indeed, this particle was selected for some inversions at the expense of the Rosette 3-bullet.

The statistical study further highlighted the previous findings and displayed promising results. As a finding, a larger number of SSPs within the 1D Bayesian inversion increases the number of successful inversions. Next, using the scattering index P_{SI} to categorize the 2-month results, it was found that mixtures are more frequent for low values. On the contrary, for a high P_{SI} index, the method tends to select only one particle. In agreement with the P_{SI} index, mixtures are preferred for low surface precipitation and low ice water path contents. Individual particles are favored for high values of surface precipitation and ice water path contents. One perspective of this study would be to categorize the inversion results with different parameters. The convective/stratiform parameters and environmental fields being closely related to microphysical properties could help to gain an understanding of the SSP choices.

This study demonstrated the feasibility and interest in using several SSPs for the inversion of cloudy microwave radiances at larger frequencies. Compared to the other methods (Baran & Labonnote, 2007; Kulie et al., 2010; Ringerud et al., 2019), this approach has the advantage of dynamically building a mixture of SSP by using microwave observations as an a priori information. Experiments using this revised 1D Bayesian method will be undertaken to assimilate cloudy and/or precipitating Bts from the GMI microwave radiometer.

AUTHOR CONTRIBUTIONS

Marylis Barreyat: Conceptualization; investigation; methodology; visualization; writing – original draft; writing – review and editing. **Philippe Chambon:** Conceptualization; investigation; methodology; funding acquisition; project administration; resources; supervision; writing – review and editing. **Jean-François Mahfouf:** Conceptualization; investigation; methodology; supervision; writing – review and editing. **Ghislain Faure:** Conceptualization; investigation; methodology; supervision; writing – review and editing.

ACKNOWLEDGEMENTS

This research is funded by Météo-France and Région Occitanie (PhD grant for Marylis Barreyat). The authors acknowledge the Centre National d'Études Spatiales (CNES) for the financial support of this scientific research activity part of ≪the Infrarouge, Micro-Ondes et Transfert radiatif ensembliste pour la prévision des Extrêmes de Précipitations≫ (IMOTEP) project. The authors also want to thank Christophe Accadia and Yves Bouteloup for their useful advice.

FUNDING INFORMATION

This research is funded by Météo-France and Région Occitanie (PhD grant for Marylis Barreyat). The authors acknowledge the Centre National d'Études Spatiales (CNES) for the financial support of this scientific research activity part of the Infrarouge, Micro-Ondes et Transfert radiatif ensembliste pour la prévision des Extrêmes de Précipitations (IMOTEP) project.

ORCID

Marylis Barreyat https://orcid.org/0000-0002-1502-3120

REFERENCES

Baran, A.J. & Labonnote, L.C. (2007) A self-consistent scattering model for cirrus. I: the solar region. *Quarterly Journal of the Royal Meteorological Society: A Journal of the Atmospheric Sciences, Applied Meteorology and Physical Oceanography*, 133(629), 1899–1912.

Barreyat, M., Chambon, P., Mahfouf, J.F., Faure, G. & Ikuta, Y. (2021) A 1D Bayesian inversion applied to GPM microwave imager observations: sensitivity studies. *Journal of the Meteorological Society of Japan. Ser. II*, 99(4), 1045–1070.

Barton, N., Metzger, E.J., Reynolds, C.A., Ruston, B., Rowley, C., Smedstad, O.M. et al. (2021) The Navy's Earth System Prediction Capability: a new global coupled atmosphere-ocean-sea ice prediction system designed for daily to subseasonal forecasting. *Earth and Space Science*, 8(4), e2020EA001199.

Brath, M., Ekelund, R., Eriksson, P., Lemke, O. & Buehler, S.A. (2020) Microwave and submillimeter wave scattering of oriented ice particles. *Atmospheric Measurement Techniques*, 13(5), 2309–2333.

Caumont, O., Ducrocq, V., Wattrelot, É., Jaubert, G. & Pradier-Vabre, S. (2010) 1D+3DVar assimilation of radar reflectivity data: a proof of concept. *Tellus A: Dynamic Meteorology and Oceanography*, 62(2), 173–187.

Ding, J., Bi, L., Yang, P., Kattawar, G.W., Weng, F., Liu, Q. et al. (2017) Single-scattering properties of ice particles in the microwave regime: temperature effect on the ice refractive index with implications in remote sensing. *Journal of Quantitative Spectroscopy and Radiative Transfer*, 190, 26–37.

Duruisseau, F., Chambon, P., Wattrelot, E., Barreyat, M. & Mahfouf, J.F. (2019) Assimilating cloudy and rainy microwave observations from SAPHIR on board Megha Tropiques within the ARPEGE global model. *Quarterly Journal of the Royal Meteorological Society*, 145(719), 620–641.

Eriksson, P., Ekelund, R., Mendrok, J., Brath, M., Lemke, O. & Buehler, S.A. (2018) A general database of hydrometeor single

scattering properties at microwave and sub-millimetre wavelengths. *Earth System Science Data*, 10(3), 1301–1326.

Faure, G., Chambon, P. & Brousseau, P. (2020) Operational implementation of the AROME model in the tropics: multiscale validation of rainfall forecasts. *Weather and Forecasting*, 35(2), 691–710.

Field, P.R., Heymsfield, A.J. & Bansemer, A. (2007) Snow size distribution parameterization for midlatitude and tropical ice clouds. *Journal of the Atmospheric Sciences*, 64(12), 4346–4365.

Geer, A. & Baordo, F. (2014) Improved scattering radiative transfer for frozen hydrometeors at microwave frequencies. *Atmospheric Measurement Techniques*, 7(6), 1839–1860.

Geer, A., Baordo, F., Bormann, N., Chambon, P., English, S., Kazumori, M. et al. (2017) The growing impact of satellite observations sensitive to humidity, cloud and precipitation. *Quarterly Journal of the Royal Meteorological Society*, 143(709), 3189–3206.

Geer, A.J. (2021) Physical characteristics of frozen hydrometeors inferred with parameter estimation. *Atmospheric Measurement Techniques*, 14(8), 5369–5395. Available from: https://doi.org/10.5194/amt-14-5369-2021

Grody, N.C. (1991) Classification of snow cover and precipitation using the special sensor microwave imager. *Journal of Geophysical Research: Atmospheres*, 96(D4), 7423–7435.

Guerbette, J., Mahfouf, J.F. & Plu, M. (2016) Towards the assimilation of all-sky microwave radiances from the SAPHIR humidity sounder in a limited area NWP model over tropical regions. *Tellus A: Dynamic Meteorology and Oceanography*, 68(1), 28620.

Haddad, Z., Steward, J., Tseng, H.C., Vukicevic, T., Chen, S.H. & Hristova-Veleva, S. (2015) A data assimilation technique to account for the nonlinear dependence of scattering microwave observations of precipitation. *Journal of Geophysical Research: Atmospheres*, 120(11), 5548–5563.

Hallett, J. & Mason, B.J. (1958) The influence of temperature and supersaturation on the habit of ice crystals grown from the vapour. *Proceedings of the Royal Society of London Series A: Mathematical and Physical Sciences*, 247(1251), 440–453.

Hong, G. (2007) Parameterization of scattering and absorption properties of nonspherical ice crystals at microwave frequencies. *Journal of Geophysical Research: Atmospheres*, 112(D11).

Kidd, C., Matsui, T., Chern, J., Mohr, K., Kummerow, C. & Randel, D. (2016) Global precipitation estimates from cross-track passive microwave observations using a physically based retrieval scheme. *Journal of Hydrometeorology*, 17(1), 383–400.

Kidd, C., Matsui, T. & Ringerud, S. (2021) Precipitation retrievals from passive microwave cross-track sensors: the precipitation retrieval and profiling scheme. *Remote Sensing*, 13(5), 947.

Kneifel, S., Neto, J.D., Ori, D., Moisseev, D., Tyynelä, J., Adams, I.S. et al. (2018) Summer snowfall workshop: scattering properties of realistic frozen hydrometeors from simulations and observations, as well as defining a new standard for scattering databases. *Bulletin of the American Meteorological Society*, 99(3), ES55–ES58. Available from: https://journals.ametsoc.org/view/journals/bams/99/3/bams-d-17-0208.1.xml

Kulie, M.S., Bennartz, R., Greenwald, T.J., Chen, Y. & Weng, F. (2010) Uncertainties in microwave properties of frozen precipitation: implications for remote sensing and data assimilation. *Journal of the Atmospheric Sciences*, 67(11), 3471–3487.

Kummerow, C., Hong, Y., Olson, W., Yang, S., Adler, R., McCollum, J. et al. (2001) The evolution of the Goddard Profiling Algorithm (GPROF) for rainfall estimation from passive microwave sensors. *Journal of Applied Meteorology*, 40(11), 1801–1820.

Liu, G. (2008) A database of microwave single-scattering properties for nonspherical ice particles. *Bulletin of the American Meteorological Society*, 89(10), 1563–1570.

Magono, C. & Lee, C.W. (1966) Meteorological classification of natural snow crystals. *Journal of the Faculty of Science, Hokkaido University. Series 7, Geophysics*, 2(4), 321–335.

Mangla, R., Indu, J., Chambon, P. & Mahfouf, J.F. (2021) First steps towards an all-sky assimilation framework for tropical cyclone event over Bay of Bengal region: evaluation and assessment of GMI radiances. *Atmospheric Research*, 257, 105564.

Marshall, J.S. & Palmer, W.M.K. (1948) The distribution of raindrops with size. *Journal of Atmospheric Sciences*, 5(4), 165–166. Available from: https://doi.org/10.1175/1520-0469(1948)005<0165:TDORWS>2.0.CO;2

Nakaya, U. (1954) *Formation of snow crystals*, Vol. 3. Cambridge: Harvard University Press.

Petty, G.W. & Huang, W. (2011) The modified gamma size distribution applied to inhomogeneous and nonspherical particles: key relationships and conversions. *Journal of the Atmospheric Sciences*, 68(7), 1460–1473.

Randel, D.L., Kummerow, C.D. & Ringerud, S. (2020) The Goddard Profiling (GPROF) precipitation retrieval algorithm. In *Satellite precipitation measurement*. Cham: Springer, pp. 141–152.

Ricard, D., Lac, C., Riette, S., Legrand, R. & Mary, A. (2013) Kinetic energy spectra characteristics of two convection-permitting limited-area models AROME and Meso-NH. *Quarterly Journal of the Royal Meteorological Society*, 139(674), 1327–1341.

Riccardi, U., Tammaro, U. & Capuano, P. (2021) Tropospheric delay in the Neapolitan and Vesuvius Areas (Italy) by means of a dense GPS array: a contribution for weather forecasting and climate monitoring. *Atmosphere*, 12(9), 1225.

Ringerud, S., Kulie, M.S., Randel, D.L., Skofronick-Jackson, G.M. & Kummerow, C.D. (2019) Effects of ice particle representation on passive microwave precipitation retrieval in a Bayesian scheme. *IEEE Transactions on Geoscience and Remote Sensing*, 57(6), 3619–3632.

Saunders, R., Hocking, J., Turner, E., Rayer, P., Rundle, D., Brunel, P. et al. (2018) An update on the RTTOV fast radiative transfer model (currently at version 12). *Geoscientific Model Development*, 11(7), 2717–2737.

Thrun, M.C., Gehlert, T. & Ultsch, A. (2020) Analyzing the fine structure of distributions. *PLoS One*, 15(10), e0238835.

Wattrelot, E., Caumont, O. & Mahfouf, J.F. (2014) Operational implementation of the 1D+ 3D-Var assimilation method of radar reflectivity data in the AROME model. *Monthly Weather Review*, 142(5), 1852–1873.

Wilheit, T., Kummerow, C.D. & Ferraro, R. (2003) NASDARainfall algorithms for AMSR-E. *IEEE Transactions on Geoscience and Remote Sensing*, 41(2), 204–214.

How to cite this article: Barreyat, M., Chambon, P., Mahfouf, J.-F., & Faure, G. (2022). A 1D Bayesian inversion of microwave radiances using several radiative properties of solid hydrometeors. *Atmospheric Science Letters*, e1142. https://doi.org/10.1002/asl.1142